

PCCP

Accepted Manuscript



This is an *Accepted Manuscript*, which has been through the Royal Society of Chemistry peer review process and has been accepted for publication.

Accepted Manuscripts are published online shortly after acceptance, before technical editing, formatting and proof reading. Using this free service, authors can make their results available to the community, in citable form, before we publish the edited article. We will replace this *Accepted Manuscript* with the edited and formatted *Advance Article* as soon as it is available.

You can find more information about *Accepted Manuscripts* in the [Information for Authors](#).

Please note that technical editing may introduce minor changes to the text and/or graphics, which may alter content. The journal's standard [Terms & Conditions](#) and the [Ethical guidelines](#) still apply. In no event shall the Royal Society of Chemistry be held responsible for any errors or omissions in this *Accepted Manuscript* or any consequences arising from the use of any information it contains.

CW-Laser-Induced Morphological Changes of a Single Gold Nanoparticle on Glass: Observation of Surface Evaporation[†]

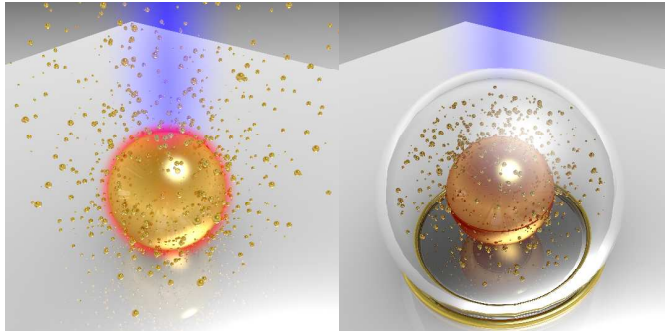
Kenji Setoura, Yudai Okada, and Shuichi Hashimoto*

Department of Optical Science and Technology, The University of Tokushima, Tokushima
770-8506, Japan

* Corresponding author: E-mail: hashichem@tokushima-u.ac.jp

[†] Electronic supplementary information (ESI) is available

Graphical abstract 4 × 8 cm



CW laser illumination of a single gold nanoparticle enables surface evaporation resulting in controlled size-reduction that depends on laser intensity. (20 words)

Abstract

Pulsed-laser heating of colloidal noble-metal nanoparticles in an aqueous solution induces morphological changes such as size reduction. However, the technique suffers disadvantages through polydispersed products. Here, we show that continuous-wave (CW) laser heating of single gold nanoparticles is capable of generating particles of smaller diameters with superb control in terms of exposure time and intensity. We show, based on calculations of particle temperatures under illumination, that surface evaporation below the boiling point of bulk gold occurs, resulting in a gradual diameter decrease in air. In our experiment, a focused illumination of Au NPs through an objective lens of a microscope provided peak-power densities (10^6 – 10^7 W cm⁻²) equivalent to that of a typical nanosecond laser. Nevertheless the heating rate under CW laser illumination is much lower than that under pulsed-laser illumination, resulting in better control over nanoparticle heating and related morphological changes. Furthermore, the single-particle study of such heating helps us to clarify the evolution of such changes to a given particle by regulating the laser intensity.

Keywords: photothermal evaporation, CW laser heating, size reduction, bubble formation, temperature calculation

1. Introduction

Photothermal properties of plasmonic nanoparticles (NPs) and nanostructures have attracted increasing attention because of potential applications to various fields including cancer therapy, bioimaging, drug delivery, and nanofabrication.¹⁻⁵ The photothermal response arises because illuminating the NP with visible light enables the excitation of its localized surface plasmon resonance (LSPR) band, leading to an extremely efficient extinction (absorption and scattering) of incident light.⁶⁻⁸ The light absorption results in an increase in particle temperature caused by the LSPR decay in which excited electrons couple with phonons within the NP. The generated thermal energy is quickly transferred to the NP environment through phonon-phonon coupling, contributing to local heating of the area surrounding the particle.^{2,5,9-11}

Previously, continuous-wave (CW) laser heating of Au NPs was used for material fabrications,¹² and particle manipulation^{13,14} and also light manipulation.¹⁵ Laser intensities of 10^4 – 10^6 W cm⁻² that realize high local temperatures (~100°C or higher) were employed in applications such as embossing and polymer-film milling by manipulating a single Au NP,^{16,17} fabricating a nanohole on a glass substrate,¹⁸ and allowing nanoscale phase transition of phospholipids membranes through heating an Au NP.^{19,20} Laser powers as in material fabrication were used for a photothermal single-particle imaging of small Au NPs (5–20 nm).^{21,22} CW laser illuminations with such high intensities can cause modifications in particle morphology. Indeed, recently, 100–150-nm-diameter Au nanospheres supported on a glass substrate in air were demonstrated to undergo surface melting under the illumination of a 532-nm or 488-nm CW laser beam with peak-power densities of 1.5 – 6×10^5 W cm⁻², leading to particle temperatures above 550 K.²³

Noticeable changes in particle morphology, such as reshaping from rod to sphere and particle size reduction, have been realized by exposing plasmonic nanoparticles to high-intensity pulsed-lasers with peak-power densities of 10^7 – 10^{12} W cm⁻².^{5,24} However, it has rarely been investigated whether CW laser irradiation can cause large modifications, in for example particle

size, besides surface melting, for Au NPs without resorting to pulsed lasers. The CW laser irradiation has advantages over pulsed-laser irradiation because this method precludes the involvement of non-photothermal and multi-photon absorption-induced ablations, and thus purely photothermal process can be singled out. The equilibrium particle temperature under CW laser exposure is reached in less than $\sim 1 \mu\text{s}$ and particle temperatures during the irradiation can be estimated provided that information such as the absorption cross-section, C_{abs} of a NP, laser intensity, I and the thermal conductivity of the medium, k_{med} is given.²⁵ Moreover, the particle temperature at which a particular morphological change is initiated can be determined experimentally.^{23,26} Traditionally, temperatures above the boiling point (bp) are considered to be prerequisites for photothermal evaporation.²⁷⁻²⁹ In analogy with surface melting that takes place at temperatures below the melting point (mp),²³ our interest is turned to surface evaporation that may take place below the bulk bp of ~ 3100 K. Such a possibility has been suggested recently for homogeneous heating.³⁰⁻³²

For our purpose, a single-particle study is best suited rather than ensemble measurements.³³ Ensemble measurements suffer a drawback in that both non-irradiated and irradiated particles are observed at various spatial laser intensities in postmortem analyses. Additionally, the finite size distribution of the original particles is a problem. The single-particle approach is favored in our study because it gives an exact and precise picture of a laser-induced event. Some confusing ensemble measurements have been reported in the literature. While one study reported no femtosecond-laser-induced fragmentation of Au NPs dispersed in aqueous solution, another study demonstrated its occurrence.^{34,35} This discrepancy arises presumably because of the difficulty in identifying the small number of irradiation products present in the vast majority of intact reactants. We note that the pulsed-laser fixation and ablation studies of Au NPs at a single-particle level have been performed by Ito and coworkers.^{36,37}

In this study, we present optical spectroscopy and scanning electron microscopy (SEM) measurements on the morphological changes of a single Au NP initiated by a focused 488-nm CW

laser excitation. A temperature simulation was also performed that supported the experiment analysis. We observed a controlled size reduction describable as layer-by-layer stripping distinct from the uncontrolled destructive ablation observed previously for nanosecond-pulsed-laser excitation.^{27,28,37} Apart from surface melting, we observed surface evaporation taking place below the *bp*. Particle modifications caused by laser-induced surface evaporation have had less attention in the past.

2. Experimental

Aqueous solutions of Au NPs with nominal diameters of 100 nm (cat. #: EMGC100) were purchased from BBI Solutions (Cardiff, UK). The particles were synthesized using a variation of the Frens citrate reduction method, and were stabilized with citrate.³⁸ The particles were transformed to spherical shape from their original faceted shape by irradiating with weak-intensity nanosecond laser pulses of wavelength 532 nm ($\sim 10 \text{ mJ cm}^{-2}$). The particle image acquired using a transmission electron microscope and the corresponding size distribution ($102 \pm 4 \text{ nm}$) are given in ESI, Fig. S1. The Au NPs were spin-coated onto a 24 mm \times 24 mm \times 0.5 mm cover slip (D263T, Matsunami, Osaka, Japan) cleansed in a plasma reactor (YHS-R, Sakigake, Japan; 70 W, 20 kHz) for 40 s on each side. The Au NPs were washed three times with double-distilled water by placing 0.5 mL of water on a spin coater and spun. Aside from this sample preparation referred to as air/glass, Au NPs on the glass slide were immersed in water in a 90- μL chamber consisting of two cover slips sandwiched with a 0.3-mm-thick silicone rubber spacer referred to as water/glass.

The laser illumination of a single Au NP was performed using an objective lens (60 \times , NA = 0.70) of an inverted microscope (IX 71, Olympus, Japan; equipped with a dark-field condenser U-DCD (NA = 0.8–0.92)) with two output ports (see ESI, S2 for an illustration of the experimental setup with typical microscope images of single Au NPs). The output from one port was relayed to a spectrograph consisting of a polychromator (SP300i, Acton Research Corp., Acton, MA; grating: 150 grooves/mm, blazed at 500 nm) and a CCD camera (type: DU401-BR-DD, Andor Technology,

Belfast, UK; operated at -60°C) through a $300\text{-}\mu\text{m}$ -diameter pinhole, while the output from the other port was used for imaging with a digital camera (DS-5M, Nikon Digital Sight, Kanagawa, Japan). The dark-field microscopy-spectroscopy was used to select a single particle to be subjected later to laser illumination. The particles were brought to the laser spot by scanning with a sample chamber on a motorized stage (BIOS-105T, SigmaKoki, Tokyo, Japan; 100-nm resolution). The excitation of a single Au NP was performed using a focused beam from a 488-nm CW laser (OBIS-488-LX-150, Coherent Inc., Santa Clara, CA). We used a 488-nm wavelength because this excitation wavelength is slightly off-set from the LSPR peak position and the absorption-cross section is unaffected by temperature changes. In contrast, the LSPR peak intensity is strongly dependent on the particle temperature and medium refractive index changes (ESI, Fig.S3). The excitation of the LSPR band causes the value of absorption cross-section (C_{abs}) for NPs to decrease with increasing temperature because of temperature-induced damping, making it difficult to estimate the particle temperature. The irradiation periods were controlled by applying mechanical shutters (F77, Suruga SEIKI Co. Ltd., Tokyo, Japan; F100, Nikon Digital Sight, Kanagawa, Japan). The laser power was measured using a photodiode power meter (OPHIR, Orion). The spatial laser profile was determined from scattering-signal intensity measurements from the 100-nm -diameter Au NP while scanning with the stage at a 100-nm interval. The laser beam diameter thus determined was $1.2\ \mu\text{m}$ although a calculated $1/e^2$ diameter of $0.5\ \mu\text{m}$ was obtained assuming a Gaussian beam profile and using experimental optical parameters ($\text{NA} = 0.70$, $\lambda = 488\ \text{nm}$, $n = 1.33$). The laser peak-power density I_p ($\text{mW}\ \mu\text{m}^{-2}$) can be expressed as²³

$$I_p = \frac{P(2.3546)^2}{2\pi(\text{FWHM})^2} \quad (1)$$

where P is the power density of the laser (measured laser power divided by beam area).

We measured the single-particle scattering spectra of Au NPs before and after a set duration for laser illumination to observe optical spectral changes associated with the morphological changes

of particles.²³ We also took particle images using SEM after each irradiation. In our experiment, it was not possible to obtain SEM images before and after irradiation for the same particle. Therefore, we selected particles of similar diameters for laser excitation by examining peak positions in the scattering spectra: particles with peak positions, 540 ± 1 nm in air/glass and 579 ± 2 nm in water/glass, were illuminated. For SEM measurements, we inspected at least 10 particles to minimize statistical errors.

A field-emission electron microscope (S4700, Hitachi, Tokyo, Japan) was used for imaging the particles. For imaging of the particles on glass substrates, Pt-Pd alloy was sputter-deposited; by measuring the thickness of the film on a glass substrate at various locations, the thickness was determined to be 5 ± 2 nm for 100-nm Au NPs. For postmortem SEM imaging, each single Au NP irradiated was located using an optical microscope; the glass substrates were patterned using femtosecond laser irradiation.

Estimations of the particle temperature of citrate-capped Au NPs under CW laser illumination were performed based on a one-dimensional (1D) heat conduction equation using experimentally determined, effective thermal conductivities, k_{eff} , of the medium and substrate.²⁶ The method reportedly can estimate particle temperatures between 300 and 700 K with an accuracy of ± 20 K.

3. Results and discussion

The CW-laser excitation of an Au NP supported on a glass substrate and exposed to the surrounding medium enables the particle temperature, T_p to increase with laser-energy absorption. Simultaneously, heat conduction from particle to medium as well as to the substrate takes place resulting in thermal equilibration.²⁶ An equilibrium temperature is assumed to be reached within less than a microsecond (ESI, Fig. S4). In our experiment, the laser illumination was performed through the objective lens of a microscope for spherical single Au NPs (102 ± 4 nm) exposed to air or immersed in a water chamber. The spectral peak position of the scattered white light from a single Au NP was used in selecting target particles of similar sizes before irradiation; the scattering

spectra were used to evaluate the morphological changes due to irradiation. We describe below the observed heating effect on exposure to 488-nm laser light.

3.1 Morphological changes in air.

Figure 1a shows the spectral changes in scattered light for single Au NPs before and after illumination for 10 ms.

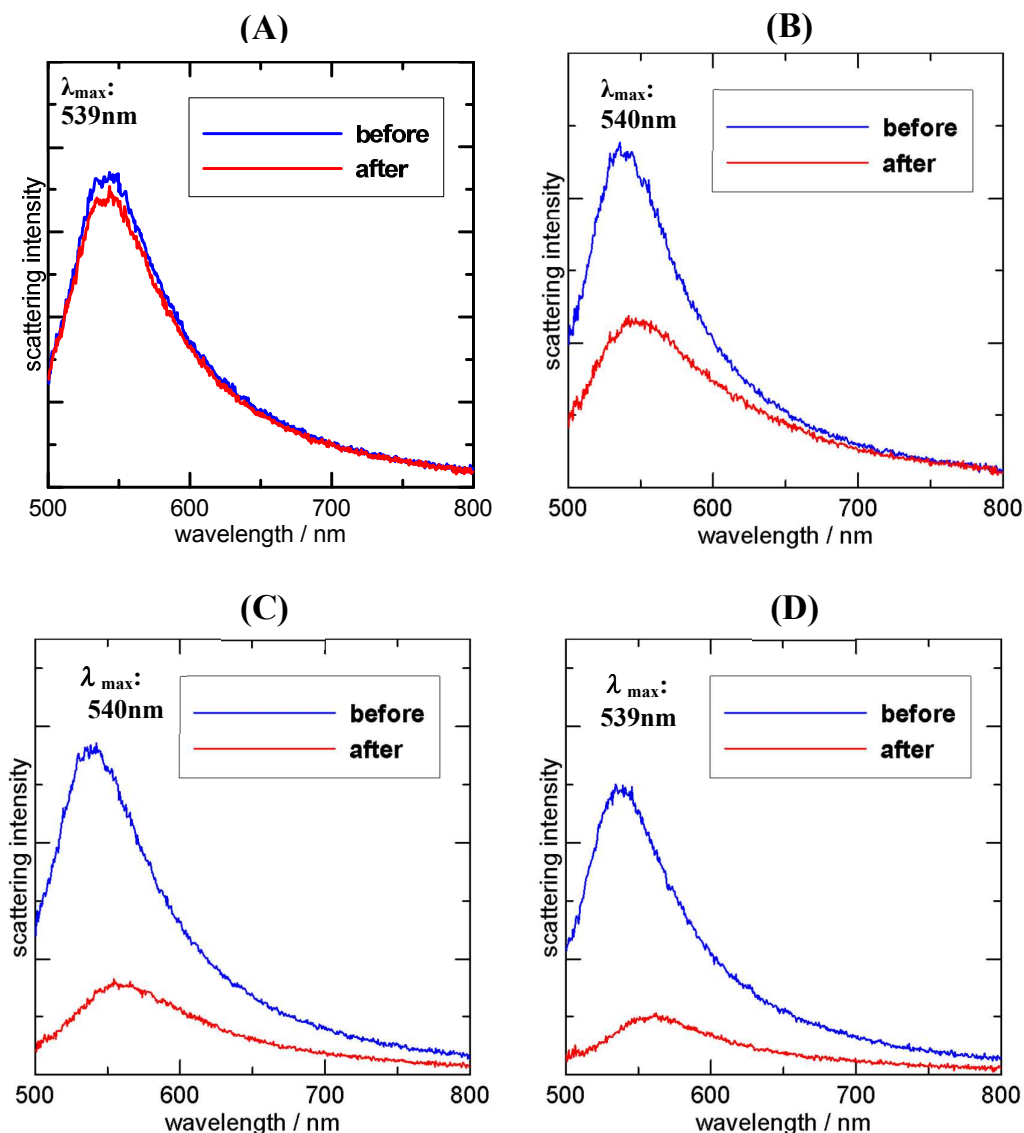


Fig. 1 (a). Scattering spectral changes of single Au NPs in air on a glass substrate after 10-ms illumination of 488-nm CW laser, focused with an objective lens (60 \times , NA: 0.70) and various laser peak-power densities: (A) 10 mW μm^{-2} , (B) 20 mW μm^{-2} , (C) 30 mW μm^{-2} , and (D) 40 mW μm^{-2} . Note that 1.0 mW μm^{-2} = 10^5 W cm^{-2} = 10^9 W m^{-2}

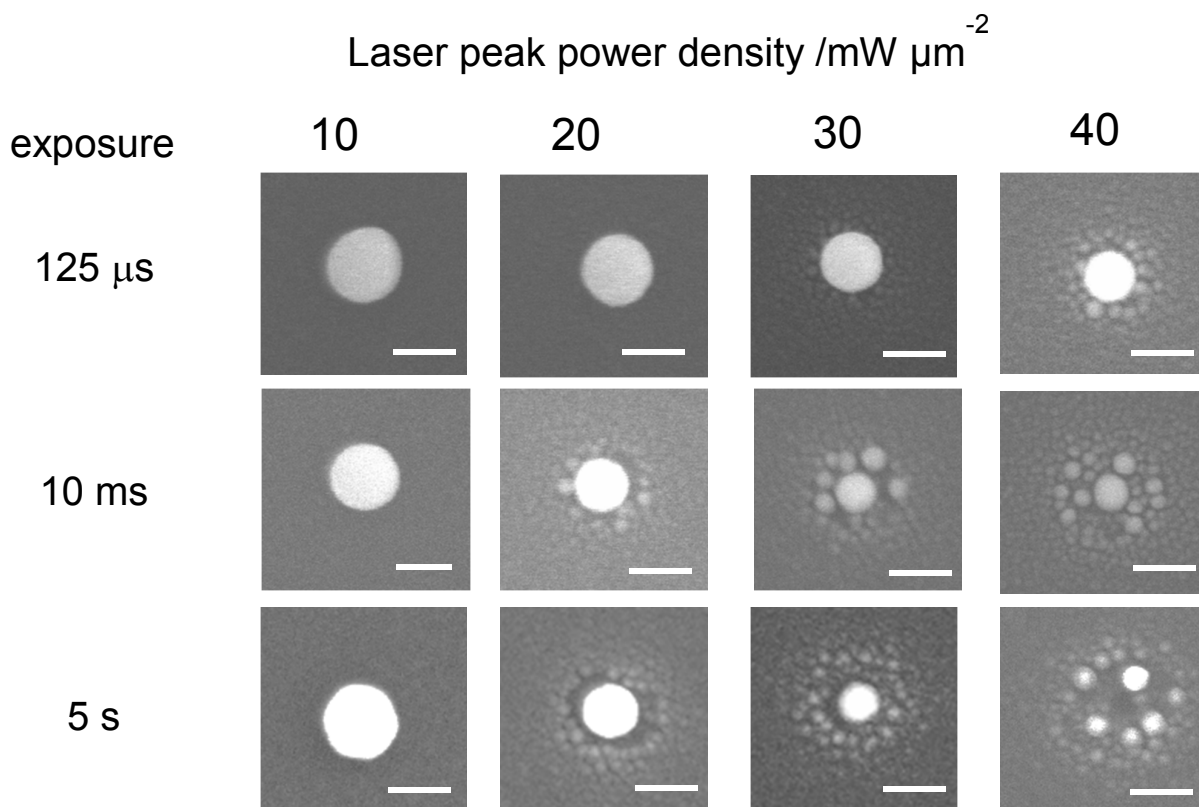


Fig. 1 (b). A typical series of SEM images of single Au NPs in air on a glass substrate captured after illumination of various durations (125 μs , 10 ms, and 5 s) with a 488-nm CW laser at the same peak-power densities and focused with the same objective lens. Scale bars: 100 nm.

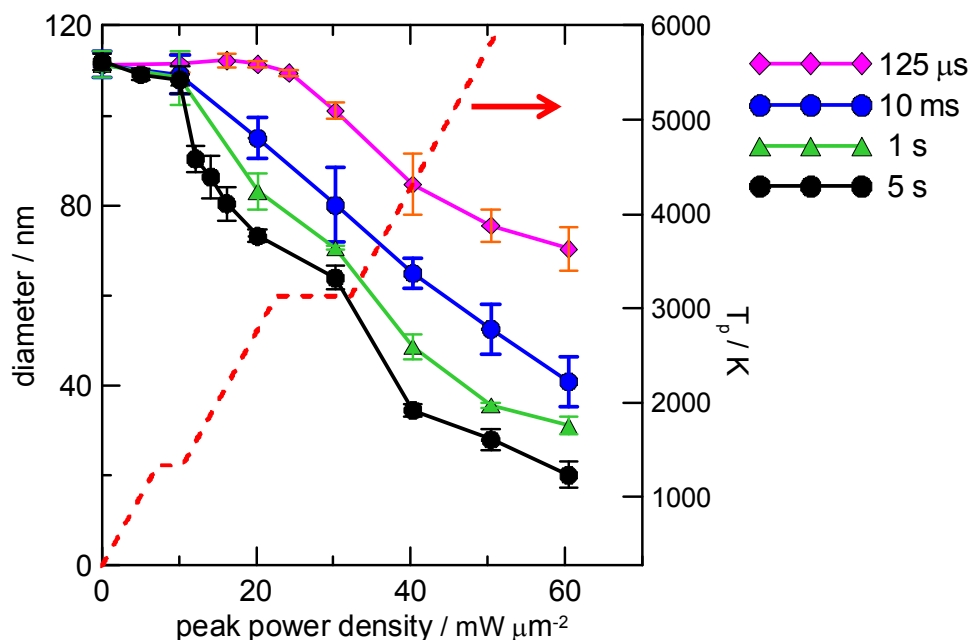


Fig. 1 (c). Average particle diameter as a function of laser peak-power density in air. Four descending curves (scale: left) were constructed from SEM images similar to those in Fig. 1(b). The particle temperature, T_p as a function of laser peak-power density (ascending dashed red line; scale: right) was calculated using a 1D heat conduction equation (ESI, S5). The two plateaus correspond to the melting and boiling enthalpies. The particle diameters shown include the sputter-deposited Pt–Pd layer of 5 ± 2 nm. The average initial Au diameter was 112 ± 4 nm.

Below $10 \text{ mW } \mu\text{m}^{-2}$, practically no scattering spectral changes were observed (Fig. 1a-A). Above $15 \text{ mW } \mu\text{m}^{-2}$, however, the light scattering intensity decreased notably with increasing laser power density. Concurrently, scattering spectral red-shifts occurred, the size of which slightly depends on the laser intensities. The former observation suggests that particles of greater diameter decrease under higher laser intensity because the light scattering intensity scales as the 6-th power of the diameter.⁷ The latter observation suggests that the occurrence of particle-particle interaction after irradiation because plasmon-plasmon interaction through particle association has been known to cause red-shifts in LSPR peak positions.^{39,40} Overall, the observed spectral changes suggest that

with increasing laser intensity a greater size reduction takes place with the simultaneous formation of associated structures of particles. Light scattering spectroscopy also suggested that a greater size reduction resulted with longer exposure periods (not shown). Although the optical scattering measurement is available for quick assessment of single particle event, detailed information regarding the particle morphological changes cannot be extracted from only this measurement. Thus, we recorded SEM images associated with the laser illumination.

Figure 1b shows a typical series of SEM images after illumination of various durations at different laser intensities. Strong morphological changes are seen to occur, that produce a size-reduced core surrounded by much smaller satellites. Importantly, the core size reduced gradually with increasing laser intensity and also increasing irradiation period. Figure 1c shows a graph summarizing particle core diameters plotted as a function of laser peak-power density at various illumination periods; particle diameters were extracted from the SEM images similar to those in Fig. 1b. The four descending curves dependent on the exposure periods obtained from data points were extracted from SEM images. Exposing the same particle more than once for a postmortem SEM acquisition was not possible, therefore, we used different particles of similar diameters for the series of images. Figure 1c clearly shows the laser intensity- and irradiation period-dependent decreases in the original particle diameters.

Figure 1c also includes the particle temperature (T_p) calculated as a function of laser peak-power density (ascending red dashed line). We used the 1D heat conduction equation to acquire laser intensity-dependent particle temperatures (ESI, S5). Previously, it was shown that T_p obtained by the application of this equation using experimentally determined effective thermal conductivity was in good agreement with both experimental and rigorous computational T_p values for various medium-substrate combinations at temperatures below 700 K.²⁶ We assumed that the slope of the I vs. T_p curves is similar at temperatures above 700 K and in liquid state because the temperature-dependence of C_{abs} is negligible at the excitation wavelength of 488 nm.²⁶ We also included melting and boiling enthalpies in determining the I vs. T_p curve. Here, the lengths of the

plateau regions were determined by dividing the enthalpies by the slope (heating rate). Comparisons of the particle temperature curves and intensity-dependent particle diameters reveal that the size reduction depends critically on the irradiation period. For 125 μs of irradiation, reductions started at the laser intensity corresponding approximately at the boiling temperature. With the irradiation period increasing from 10 ms to 5 s, the laser intensity needed to initiate the reduction gradually decreased and most importantly a diameter decrease was observed at temperatures below the bp of gold.

This is significant because the temperature curve (Fig. 1c) was calculated for a 100-nm-diameter Au NP. If the particle diameter decreases continuously because of laser illumination, T_p should also decrease because C_{abs} for Au NP decreases with particle diameter. This situation can be understood from the variation of T_p with particle diameter at three different laser intensities (Fig. 2).

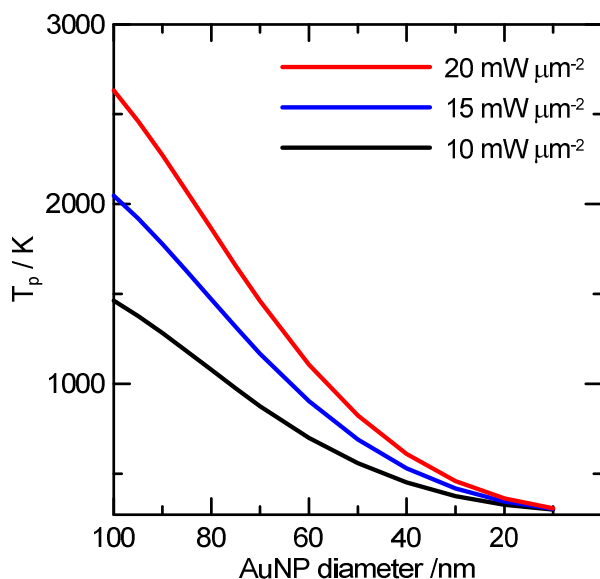


Fig. 2. Calculated particle temperatures as a function of particle diameter for three different laser peak-power densities. The particle was assumed to be supported on a glass substrate in air (effective medium refractive index: 1.12 (Ref. 23)); the excitation wavelength was 488 nm.

When we focus on the data for laser intensity of $20 \text{ mW } \mu\text{m}^{-2}$ (Fig. 1c), a gradual diameter decrease was observed with increasing illumination period after 10 ms. At this laser intensity, the initial T_p is estimated at 2650 K, which is below the bp of gold and continuous size reduction proceeded at significantly lower temperatures. After 5 s of irradiation, the particle diameter is reduced to 75 nm (70 nm without the sputtered layer) with an estimated T_p of 1500 K. In contrast, at a laser intensity of $10 \text{ mJ } \mu\text{m}^{-2}$ (Fig. 1c), no particle diameter decrease was observed even for an illumination period of 5 s; at this intensity, the estimated T_p is 1450 K, which is close to but above the mp of 1337 K for bulk gold. In terms of laser intensity, the threshold for diameter decrease is $\sim 16 \text{ mJ } \mu\text{m}^{-2}$. Accordingly, we infer that, with temperatures between mp and bp , particle diameter decreases with laser intensity as the Au NP is then a liquid droplet.

Note that at high laser intensities exceeding $35 \text{ mW } \mu\text{m}^{-2}$ at which $T_p > bp$ is estimated, rapid size changes occur for the core particles that were surrounded by many satellites. Nevertheless, a gradual laser intensity-dependent size reduction is still evident. This observation contrasts with that in a water medium where severe damage to particles was observed. Apart from the morphological changes of the particle, we observed a modification of a glass surface, specifically, the formation of a crater. Because this observation is not relevant to particle deformation, we have relegated a brief description of the changes to ESI, S6.

3.2 Morphological changes in water.

Figure 3a shows a set of SEM images after illumination in water for various durations at different laser intensities (see ESI, Fig. S7 for the corresponding scattering spectral changes).

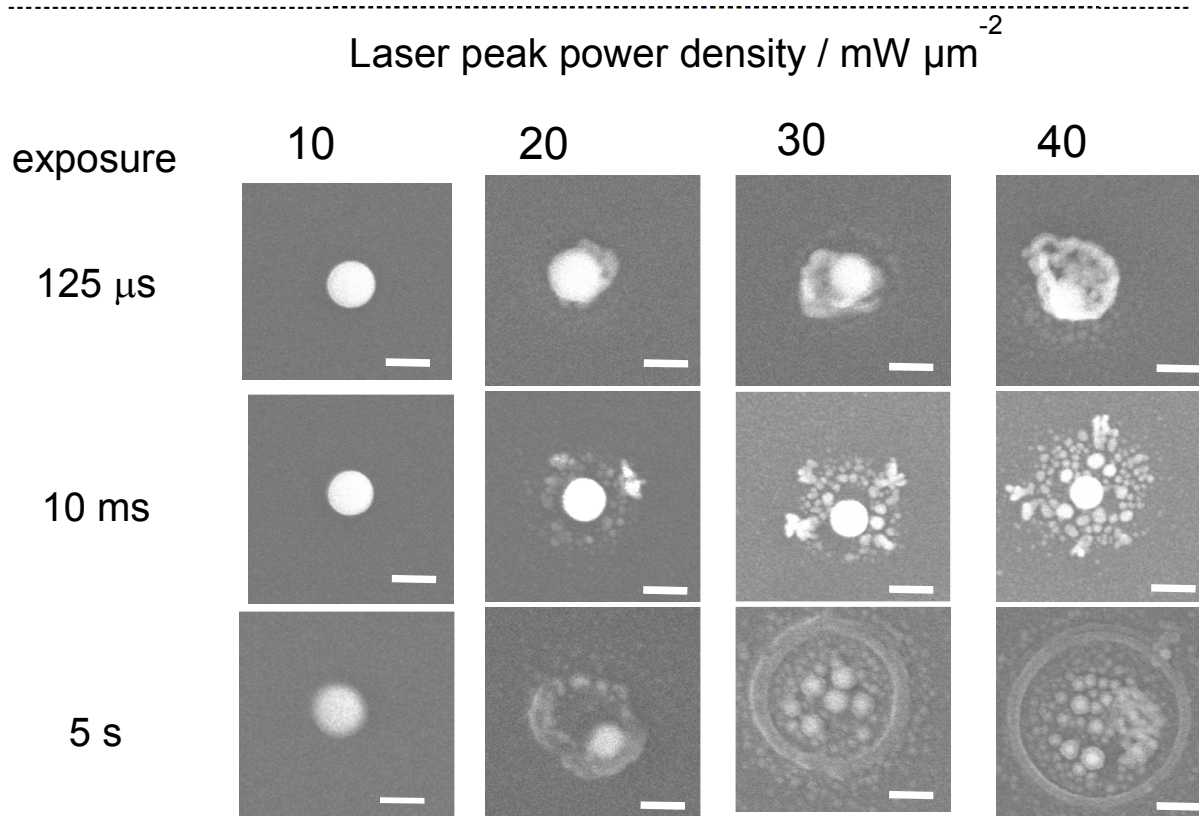


Fig. 3 (a). A series of SEM images of single Au NPs supported on a glass substrate after illumination in water over various durations (125 μs , 10 ms, and 5 s) using a CW laser at various laser peak-power densities (10, 20, 30, 40 $\text{mW } \mu\text{m}^{-2}$) and focused with an objective lens. Scale bars: 100 nm.

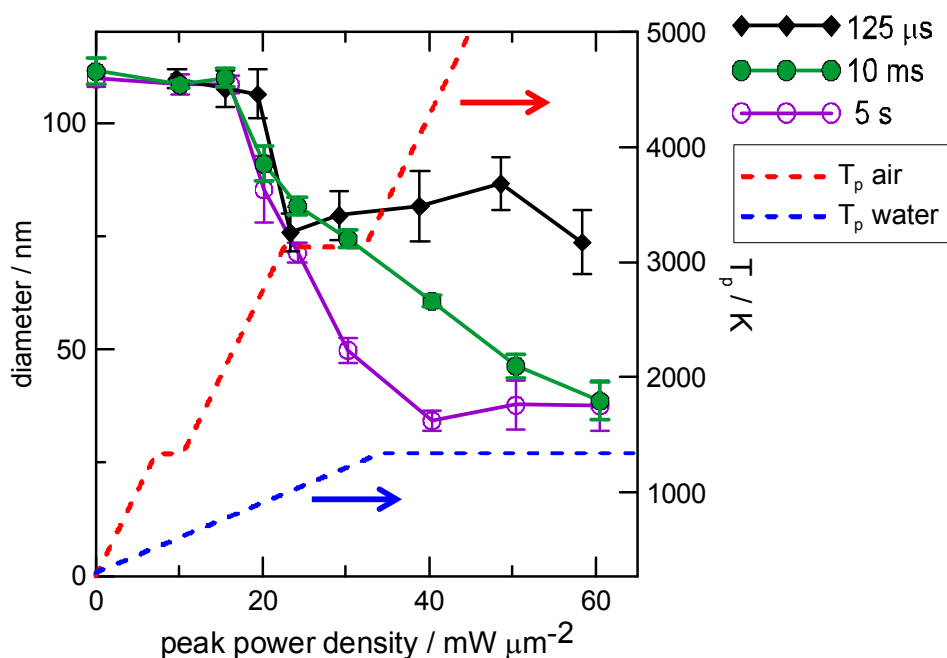


Fig. 3 (b). Average particle diameter (scale: left) as a function of laser peak-power density in water. The data for the curves is taken from SEM images in a similar manner to those in Fig. 3(a). The red dashed ascending line represents the I vs. T_p curve in air and the blue dashed ascending line is the I vs. T_p curve in water (the scale for both curves: right). The average initial Au diameter was 112 ± 4 nm including a sputter-deposited Pt-Pd layer.

The SEM images reveal morphological changes to Au NPs in water is distinct from those in air; size reduction occurred but a core particle survived, and depending on exposure periods and laser intensities, ejected products were more or less confined to those areas illuminated by the beam. For an irradiation period of 125 μs , rather than small particles observed in air, the ejected products appeared as a film that had been solidified from liquid gold droplets released from around the core of the particle. In contrast, for a 10-ms irradiation period at high intensities, explosive ejections of particle-like species from around the core were distinctly observed. The formation of a core-satellite structure is reminiscent of its observation in air, but was more confined to a smaller area in water. Furthermore, for a 5-s irradiation exposure aside from fragments, a distinct ring structure surrounding the irradiated products emerged at higher laser intensities. The ring clearly originates from the original Au particle.

A graph representing particle diameter *vs.* laser peak-power density (Fig. 3b) was constructed from an analysis of SEM micrographs (Fig. 3a). The laser intensity-dependent particle changes reveal that the threshold associated with size reduction is more clearly defined in water than in air. For instance, a threshold was observed at $20 \text{ mW } \mu\text{m}^{-2}$ for an irradiation period of $125 \mu\text{s}$ and at $16 \text{ mW } \mu\text{m}^{-2}$ for 1- and 5-s exposures. For reference, the T_p *vs.* laser peak-power density curves were calculated for Au NPs in air and water (Fig. 3b). In water, because of its greater thermal conductivity than that of air, the laser-intensity-dependent increase in T_p has a much smaller slope. Additionally, in Fig. 3b, the plateau region corresponding to the melting enthalpy consumed in water is longer than that in air because the heating rate is lower in water (see ESI, S5). Moreover, at a certain threshold laser intensity, bubble formation from the evaporation of surrounding water caused by heat transfer from the NP is known to occur.⁴¹ This can result in a sudden jump in the NP temperature surrounded by the bubble due to the poor thermal conductivity of air.⁴² Indeed, the onset of the diameter reduction observed at 1–5 s of illumination is similar to the threshold intensity of bubble formation, *i.e.*, $\sim 16 \text{ mW } \mu\text{m}^{-2}$. Here, the threshold for bubble formation was measured by the blue shift in the scattering spectrum during the 5-s excitation period.²³ Previously, a threshold of $25 \text{ mW } \mu\text{m}^{-2}$ was measured for 100-nm Au NP supported on a glass substrate immersed in water and excited with a 532-nm CW laser beam.⁴⁰ One explanation for the observed difference in our measurement is ascribed to the temperature-induced LSPR band bleaching.^{43,44}

Here, we give a scenario for particle disintegration in water. For the short exposure period of $125 \mu\text{s}$, water molecules strongly interfere with the ejection of the liquid material resulting in a film-like solid structure. The short irradiation period is insufficient to sustain the bubble expansion.⁴⁵ In contrast, for long illumination periods of 1 and 5 s, bubble formation and expansion eject gold droplets into areas where expansion ceases. With the NP sitting inside the bubble, fragmenting of the gold droplet releasing smaller droplets is possible at high temperatures. Thus, the observed confinement, expansion, and ring formation depended on laser intensity and duration. An assumption made previously⁴⁶ of whether high pressure can break up the liquid core during bubble

collapse remains unclear.

3.3 Mechanistic aspect.

Under CW laser illumination, we observed in 100-nm Au NPs a dependence of the reduced core diameter on both laser intensity and illumination period. This behavior is ascribed to the evaporation of gold droplets. In particular, we found clear evidence of evaporation occurring at temperatures below the bp of gold in air from calculations of T_p during illumination. Previously, Inasawa and coworkers observed a bimodal particle size distribution, one at 6 nm and the other at 16–24 nm, of products from the picosecond laser-induced evaporation of aqueous colloidal Au NPs with monomodal distribution of 25 ± 6 nm.³⁰ From their analysis, they proposed that the size reduction proceeds layer-by-layer at the outer surface; still, the control of particle size by ps laser illumination was unsatisfactory. Our single particle observation under CW laser illumination in air clearly showed the formation of satellite particles ejected from the remaining core particle, *i.e.*, surface evaporation, with far better core size controllability. In pulsed-laser illumination, T_p increases with time during and after illumination followed by a decrease through heat transfer to the surroundings.⁵ Thus, the photothermal evaporation takes place over a limited time interval during which T_p is above the evaporation threshold temperature. In contrast, in CW laser illumination, T_p can be kept near the evaporation threshold during the illumination period. Clearly, T_p can be better controlled by the CW laser illumination.

The size reduction of Au NPs on oxide substrates through evaporation was observed previously at temperatures far below the bulk bp of gold (~ 3100 K) when thermal treatment was applied in a furnace in an Ar atmosphere ($10\text{--}10^5$ Pa).³¹ For instance, at 950°C (1223 K) in an Ar-atmosphere at 10^5 Pa, the size reduction took place from the average diameter of 300 nm to that of 200 nm in 2 h. Furthermore, thermogravimetric analysis of Au nanorods revealed that the loss of gold starts at ~ 1200 K through evaporation.³² These observations suggest that the evaporation at temperatures below the bp of gold is possible if the heating period is sufficient. In the present study,

we found that to observe Au NP evaporation continuous heating is important.

The observed CW laser-induced evaporation of individual Au NPs is a non-isothermal event. Under constant laser illumination, C_{abs} should decrease because of a gradual decrease in NP diameter, causing a particle temperature decrease (Fig. 2). Additionally, a temperature gradient will be formed in the surrounding medium during the particle heating. From the possible 2D temperature distributions (ESI, S8) for air and water media, the temperature gradient formed in the medium acts to reduce the temperature of ejected species, which cannot occur in homogeneous heating. For non-homogeneous temperature distribution conditions, directly fitting the experimental diameter vs laser intensity curves using the evaporation model is not feasible. Instead, evaporation was simulated as follows. The rate of change in the particle radius with time, dr/dt , can be represented by^{47,48}

$$\frac{dr}{dt} = \left(\frac{M}{2\pi R \rho^2} \right)^{\frac{1}{2}} \frac{\alpha P_r}{T_p^{1/2}} \quad (2)$$

where M is the molecular weight, R is the gas constant, ρ is the density, α is the evaporation coefficient ($0 < \alpha < 1$), T_p is the particle temperature, and P_r is the vapor pressure above a particle of radius r . We calculated the diameter decrease Δr according to

$$\Delta r = \sum_{i=1}^n \left(\frac{M}{2\pi R \rho_i^2} \right)^{1/2} \frac{\alpha_s P_{r,i}}{T_{pi}^{1/2}} \Delta t_i \quad (3)$$

in which a time step Δt was set to 40 μs , P_r was taken from the literature,³¹ and α was obtained from the slope of the experimental Δr vs t curve. We first obtained C_{abs} for an initial 100-nm Au NP, then T_p was calculated, followed by acquisition of D_p (particle diameter). We repeated the same procedure using the newly obtained D_p until the final period of exposure of 1 s is reached. We only performed the calculation for air because in water a discontinuity occurs in the diameter reduction

because of bubble formation. The result (Fig. 4) shows that, at a laser intensity of $10 \text{ mW } \mu\text{m}^{-2}$, no diameter decrease occurs, whereas at 16 and $20 \text{ mW } \mu\text{m}^{-2}$, a diameter decrease is possible.

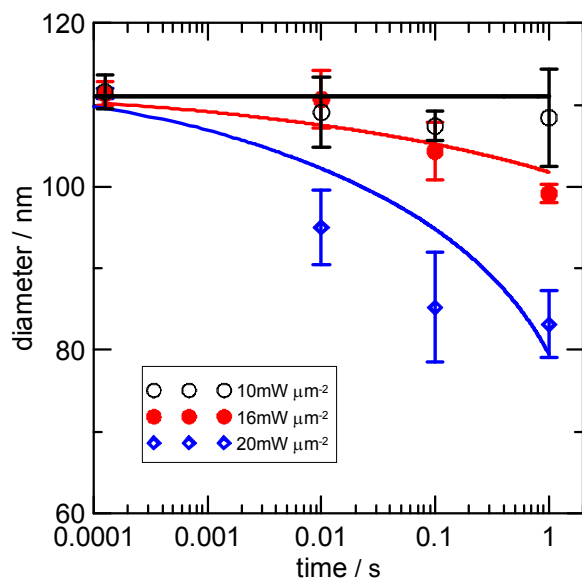


Fig. 4. Simulated particle diameter decrease in air as a function of exposure period. For comparison with experimental data, the ordinate scale was represented as the sum of the calculated diameter and the thickness of the sputter-deposited layer.

This is consistent with the observation of a threshold laser intensity of $16 \text{ mW } \mu\text{m}^{-2}$ for air. The corresponding simulation suggests that our hypothesis of evaporation below the bp of gold is qualitatively acceptable.

Note that particles generated after laser heating, i.e. cores and satellites, have spherical shapes. Previous studies on pulsed laser heating of Au NPs in solution revealed spherical products.^{18,27,30,35} Clearly liquid droplets of Au NPs undergoing evaporation tend to assume a spherical shape in minimizing their surface energy during cooling process. The observation suggests that small satellite particles formed from the condensation of evaporated species are also spherical. This suggests that the satellite particles are formed via the liquid state. Besides minimizing the surface energy, in our case, the hydrophilic glass surface may prevent liquid gold from spreading.⁴⁹ It was

also reported that simple melting of Au NPs in solution changed their appearance from faceted to spherical.⁵⁰ For supported Au NPs on substrates, laser melting was observed to induce a transformation to spherical shapes.⁵¹⁻⁵³ Thus, unless some external force is applied, deforming liquid nanodroplets into nonspherical shapes is difficult solely under the gravitational force. Interestingly, we have learned that a spherical gold nanodroplet can be deformed by an optical force to form a standing rod.⁵⁴

From the point of view of nanostructure fabrication, focused CW laser irradiation may raise the following comment. According to our temperature calculation, the surface evaporation of the 100-nm Au NP at fluences of 16–20 mW μm^{-2} occurred at temperatures from 1500 to 2650 K in air, generating cores and small fragments. However, at $20 < T_p < 30$ mW μm^{-2} where the bp of ~ 3100 K is almost reached, we observed remarkably small cores of 20–30 nm together with satellites. At still higher laser intensities, explosive evaporation similar to that occurring in high-intensity pulsed-laser excitation causes particle fragmentation. Because of the controllability of surface evaporation, the CW laser illumination provides a protocol to prepare core-satellite structures. Although various synthetic methods have been developed to prepare core-satellite structures,^{40,55,56} CW laser illumination is useful in preparing a single core-satellite structure at any location without difficulty. The CW laser illumination in water produced unusual structures, such as a ring surrounding the fragments. The structure is reminiscent of a plasmon resonator.^{57,58} Hence, CW laser-induced photothermal evaporation in water may serve to prepare structures with unusual optical properties. As mentioned above, the bubbles are responsible for the variation in Au NP evaporation although its nature has not been fully characterized. Further study is needed to reveal the critical role of bubble in particle modification.

4. Conclusion

Using CW laser illumination, we detailed the slow photothermal evaporation of Au NPs overlooked in pulsed-laser experiments. We also observed that bubble formation in water strongly affects the evaporation of Au NPs. The result suggests the need for further investigation to reveal whether bubble expansion or contraction is responsible for the fragmentation of liquid NP inside the bubble. Addressing the significance of the result, we refer to the photothermal structuring. Examples are the formation of a ring structure containing small particles, which can be useful for the development of unique plasmonic optical properties in addition to the formation of core-satellite structures with controlled sizes. When produced, the former is strongly affected by photothermal bubble formation and the latter by photothermal surface evaporation. For CW laser illumination through an objective, by regulating the irradiation period and intensity one can create unusual structures with better controllability than the pulsed-laser irradiation.

Acknowledgments

Financial support from KAKENHI (Grant Nos. 25600026 and 26286004) is gratefully acknowledged. Technical staff members, Tomoyuki Ueki and Satoshi Sugano, are acknowledged for SEM imaging.

References

1. Z. Qin and J. C. Bischof, *Chem. Soc. Rev.* 2012, **41**, 119–1217.
2. G. Baffou and R. Quidant, *Laser Photon. Rev.* 2013, **7**, 171–187.
3. E. C. Dreaden, M. A. Mackey, X. Huang, B. Kang, M. A. El-Sayed, *Chem. Soc. Rev.* 2011, **40**, 3391–3404.
4. R. Bardhan, S. Lal, A. Joshi and N. J. Halas, *Acc. Chem. Res.* 2011, **44**, 936–946.
5. S. Hashimoto, D. Werner and T. Uwada, *J. Photochem. Photobiol. C: Rev.* 2012, **13**, 28–54.
6. U. Kreibig and M. Vollmer, *Optical Properties of Metal Clusters*; Springer: Berlin, 1995.
7. C. F. Bohren and D. R. Huffman, *Absorption and Scattering of Light by Small Particles*; Wiley: New York, 1983.
8. P. Mulvaney, *Langmuir*, 1996, **12**, 788–800.
9. G. V. Hartland, *Chem. Rev.* 2011, **111**, 3858–3887.
10. A. Siems, S. A. L. Weber, J. Boneberg and A. Plech, *New J. Phys.* 2011, **13**, 043018.
11. S. Merabia, S. Shenogin, L. Joly, P. Keblinski and J. L. Barrat, *Proc. Natl. Acad. Sci. U S A* 2009, **106**, 15113–15118.
12. J. Qui, W. and G. Wei, *J. Phys. Chem. C* 2013, **118**, 20735–20749.
13. A. S. Urban, S. Carretero-Palacios, A. A. Lutich, T. Lohmüller, J. Feldmann, and F. Jäckel, *Nanoscale* 2014, **6**, 4458–4474.
14. B. Qian, D. Montiel, A. Bregulla, F. Cichos and H. Yang, *Chem. Sci.*, 2013, **4**, 1420–1429.
15. A. Heber, M. Selmke, and F. Cichos, *ACS Nano*, 2014, **8**, 1893–1898.
16. A. G. Skirtach, D. G. Kurth and H. Möhwald, *Appl. Phys. Lett.*, 2009, **94**, 093106.
17. M. Fedoruk, A. A. Lutich and J. Feldmann, *ACS Nano*, 2011, **5**, 7377–7382.
18. T. Numata, H. Tatsuta, Y. Morita, Y. Otani and N. Umeda, *IEEJ Trans.* 2007, **2**, 398–401.
19. P. M. Bendix, S. N. S. Reihani and L. B. Oddershede, *ACS Nano*, 2010, **4**, 2256–2262.
20. A. S. Urban, M. Fedoruk, M. R. Horton, J. O. Rädler, F. D. Stefani and J. Feldmann, *Nano Lett.* 2009, **9**, 2903–2908.

21. D. Boyer, P. Tamarat, A. Maali, B. Lounis and M. Orrit, *Science*, 2002, **297**, 1160–1163.
22. A. Gaiduk, P. V. Ruijgrok, M. Yorulmaz and M. Orrit, *Chem. Sci.*, 2010, **1**, 343–350.
23. K. Setoura, D. Werner and S. Hashimoto, *J. Phys. Chem. C*, 2012, **116**, 15458–15466.
24. P. Zijlstra, J. W. M. Chon and M. Gu, *Phys. Chem. Chem. Phys.* 2009, **11**, 5915–5921.
25. P. Keblinski, D. G. Cahill, A. Bodapati, C. R. Sullivan and T. A. Taton, *J. Appl. Phys.* 2006, **100**, 054305.
26. K. Setoura, Y. Okada, D. Werner and S. Hashimoto, *ACS Nano*, 2013, **7**, 7874–7885.
27. A. Takami, H. Kurita and S. Koda, *J. Phys. Chem. B* 1999, **103**, 1226–1232.
28. S. Inasawa, M. Sugiyama, S. Noda and Y. Yamaguchi, *J. Phys. Chem. B* 2006, **110**, 3114–3119.
29. D. Werner and S. Hashimoto, *J. Phys. Chem. C* 2011, **115**, 5063–5072.
30. S. Inasawa, M. Sugiyama and Y. Yamaguchi, *J. Phys. Chem. B* 2005, **109**, 9404–9410.
31. G. Meng, T. Yanagida, M. Kanai, M. Suzuki, K. Nagashima, F. Xu, Bo, Zhuge, A. Klamchuen, Y. He, S. Rahong, S. Kai and T. Kawai, *Phys. Rev. E*, 2013, **87**, 012405.
32. M. Gordel, J. Olesiak-Banska, K. Matczyszyn, C. Nogues, M. Buckleb and M. Samoc, *Phys. Chem. Chem. Phys.* 2014, **16**, 71–78.
33. P. Zijlstra and M. Orrit, *Rep. Prog. Phys.* 2011, **74**, 106401.
34. O. Warshavski, L. Minai, G. Bisker and D. Yelin, *J. Phys. Chem. C*, 2011, **115**, 3910–3917.
35. D. Werner, A. Furube, T. Okamoto and S. Hashimoto, *J. Phys. Chem. C* 2011, **115**, 8503–8512.
36. S. Ito, H. Yoshikawa and H. Masuhara, *Appl. Phys. Lett.*, 2002, **80**, 482–484.
37. S. Ito, T. Mizuno, H. Yoshikawa and H. Masuhara, *Jpn. J. Appl. Phys.* 2007, **46**, L241–243.
38. G. Frens, *Nature Phys. Sci.*, 1973, **241**, 20–22.
39. S. K. Chosh and T. Pal, *Chem. Rev.*, 2007, **107**, 4797–4862.
40. J. H. Yoon, J. Lim, and S. Yoon, *ACS Nano*, 2012, **6**, 7199–7208.
41. G. Baffou, J. Polleux, H. Rigneault and S. Monneret, *J. Phys. Chem. C*, 2014, **118**, 4890–4898.
42. Z. Fang, Y.-R. Zhen, O. Neumann, A. Polman, F. J. García de Abajo, P. Nordlander and N. J. Halas, *Nano Lett.*, 2013, **13**, 1736–1742

43. L. M. Liz-Marzan and P. Mulvaney, *New J. Chem.* 1998, **22**, 1285–1288.
44. S. Link and M. A. El-Sayed, *J. Phys. Chem. B*, 1999, **103**, 4212–4217.
45. Y. Nishimura, K. Nishida, Y. Yamamoto, S. Ito, S. Tokonami and T. Iida, *J. Phys. Chem. C*, 2014, **118**, 18799–18804.
46. C. Pitsillides, E. K. Joe, X. Wei, R. R. Anderson and C. P. Lin, *Biophys. J.*, 2003, **84**, 4023–4032.
47. J. R. Sambles, *Proc. Roy. Soc. Lond: A*. 1971, **324**, 339–351.
48. M. A. Asoro, D. Kovar and P. J. Ferreira, *ACS Nano* 2013, **7**, 7844–7852.
49. H. Sun, M. Yu, G. Wang, X. Sun and J. Lian *J. Phys. Chem. C*, 2012, **116**, 9000–9008.
50. R. E. Cavicchi, D. C. Meier, V. M. Prabhu, and S. Guha, *J. Phys. Chem. C*, 2013, **117**, 10866–10875.
51. J. Wang, Y. Chen, X. Chen, J. Hao, M. Yan, and M. Qiu, *Opt. Express*, 2011, **19**, 14726–14734.
52. M. Kawasaki and M. Hori, *J. Phys. Chem. B* 2003, **107**, 6760–6765.
53. A. Habenicht, M. Olapinski, F. Burmeister, P. Leiderer, and J. Boneberg, *Science*, 2005, **309**, 2043–2045.
54. A. Kuhlicke, S. Schietinger, C. Matyssek, K. Busch, and O. Benson, *Nano Lett.*, 2013, **13**, 2041–2046.
55. J. R. Waldeisen, T. Wang, B. M. Ross and L. P. Lee, *ACS Nano* 2011, **5**, 5383–5389.
56. N. Gandra, A. Abbas, L. Tian and S. Singamaneni, *Nano Lett.* 2012, **12**, 2645–2651.
57. F. Hao, P. Nordlander, Y. Sonnefrad, P. V. Dorpe and S. A. Maier, *ACS Nano* 2009, **3**, 643–652
58. N. Large, J. Aizpurua, V. K. Lin, S. L. Teo, R. Marty, S. Tripathy and A. Mlayah, *Opt. Express* 2011, **19**, 5587–5595.